Electronic supporting information for

Exceptional interfacial electrochemistry of few-layered 2D MoS_2 quantum sheets for high performance flexible solid-state supercapacitors

Swapnil Shital Nardekar[1], Karthikeyan Krishnamoorthy[1], Parthiban Pazhamalai[1], Surjit Sahoo[1], Vimal Kumar Mariappan[1], and Sang -Jae Kim[1,2*]

[1]Nanomaterials & system laboratory, Major of Mechatronics Engineering, Faculty of Applied Energy System, Jeju National University, Jeju-63243, South Korea.

[2]Department of Advanced Convergence Science & Technology, Jeju National University, Jeju-63243, South Korea.

Corresponding author Email: kimsangj@jejunu.ac.kr

S1 Experimental section

S1.1 Materials

The molybdenum disulfide powders (bulk) were obtained from Asbury carbon, USA. Sodium chloride (NaCl), sulphuric acid (H_2SO_4), polyvinyl alcohol (PVA) and N-Methyl-2-Pyrrolidone (NMP) were procured from Daejung metals and chemicals, South Korea. Carbon black and polyvinylidene fluoride (PVDF) was purchased from Alfa Aesar, South Korea. Carbon cloth was purchased from CeTech Fuel cell store, Texas. All the chemicals used in this work are of research-grade and used without further purification.

S1.2 Preparation of MoS_2 quantum sheets

A salt assisted mechanical milling process has been employed for the preparation of MoS_2 quantum sheet from bulk MoS_2 powders. [1] Briefly, the precursor bulk MoS_2 powders and NaCl were taken in the ratio of 1:10 in a tungsten carbide bowl and allowed to milling using tungsten carbide balls at a speed of 300 rpm for 15 h. Upon completion of the milling process, the milled powders were washed with doubly distilled water and ethanol several times to remove the salt content in the powders. The washed sample is allowed to ultrasound irradiation for 4 h to further to transform the pulverized materials into MoS_2 quantum sheets. The resulting powder is washed, dried at 80 °C and used for further characterization.

S1.3 Instrumentation

The crystallinity and phase of the MoS_2 powders was characterized using X-ray diffractometer (Empyrean) operated at 40 keV and 40 mA Cu Kα radiation. Laser Raman and mapping analysis were obtained using Lab Ram HR Evolution Raman spectrometer (Horiba Jobin-Yvon, France) with an excitation wavelength of 514 nm with an Ar^+ ion laser. The Raman mapping of MoS_2 QSs was analyzed using Lab Spec (Ver. 6.2) software. The high-resolution transmission electron micrograph (HR-TEM) for the bulk MoS_2 and MoS_2 QSs were carried out on an HR-TEM, JEOL JEM 2011, JEOL Ltd. X-ray photoelectron spectroscopy

(XPS) was used to analyze the chemical composition and state of elements present in MoS_2 via ESCA-2000, VG Microtech Ltd. using monochromatic X-ray beam source at 1486.6 eV (aluminium anode) and 14 kV to scan the sample surface. The AFM analysis was carried out using Bruker instrument with using tapping mode (cantilever PPPHCHR with tip radius: < 10 nm, brand: Nanosensors, material: highly doped silicon, force constant: ~42 N/m). The UV-Vis spectroscopy was used to analyze the absorbance range of material via UV-Vis spectrophotometer (Lambda 25 model). The zeta potential of the MoS_2 QSs was measured with Malvern zetasizer instrument. The bending testing of the device has been performed with a Bending Tester machine (JUNIL-JIBT-200). The electrochemical characterization was performed using Autolab PGSTAT302N electrochemical workstation.

S1.4 Preparation of PVA-H_2SO_4 gel electrolyte

The polymer gel electrolyte (PVA/H_2SO_4) was prepared using the method provided in the literature [2]. Briefly, 2 g of PVA was dissolved in 20 mL of distilled water using magnetic stirrer until the formation of a homogenous solution. To the formed homogenous solution, an appropriate amount of H_2SO_4 was added and allowed to stir under heat to form a clear and transparent gel. Finally, the obtained PVA/H_2SO_4 gel is allowed to cool at room temperature and used for the fabrication of supercapacitor.

S1.5 Fabrication of MoS_2 solid-state symmetric supercapacitors

Initially, MoS_2 quantum sheets (MoS_2 QSs) electrodes were prepared by grounding active material (MoS_2 QSs), carbon black and PVDF in the ratio (85:10:5) with the appropriate amount of NMP in an agate-mortar until the formation of slurry. The obtained slurry was coated on to the conductive carbon cloth (CC) substrate with an electroactive area of 1×1 cm^2 and dried at 80 °C overnight. The electroactive mass loading of the MoS_2 QSs electrode loaded on the carbon cloth is about 2 mg in each electrode. The MoS_2 quantum sheets symmetric supercapacitor (SSC) was fabricated using MoS_2 QSs electrode coated on carbon cloth as

positive and negative electrodes separated by PVA/H_2SO_4 gel electrolyte. The electrochemical characterization of the fabricated SSC was examined via cyclic voltammetry (CV), galvanostatic charge-discharge analyses and Electrochemical impedance spectroscopy (EIS) using an Autolab PGSTAT302N electrochemical workstation.

S1.6 Electrochemical analysis

The specific device capacitance (*Csp*) of the MoS_2 QSs SSC device was calculated from the CV and CD analysis using relation[3]:

$$C_{sp} = \int IdV / (s \times \Delta V \times M) \quad \text{..... (1)}$$

$$C_{sp} = (I \times \Delta t) / (\Delta V \times M) \quad \text{…..... (2)}$$

Here "C_{sp}" is the specific device capacitance (F g^{-1}) of MoS_2 QSs SSC device, "*I*" is the current (A), "*s*" is the scan rate (mV s^{-1}), "ΔV" is the voltage window (V), "Δt" is the discharge time (s) and "*M*" is the mass of the electrodes (mg).

The energy (*E*) and power (*P*) density of the MoS_2 QSs SSC device are calculated using the relations [4]:

$$E = 0.5 \times C_{sp} \times \Delta V^2 \text{ …… (3)}$$

$$P = E / \Delta t \text{ ……..…… (4)}$$

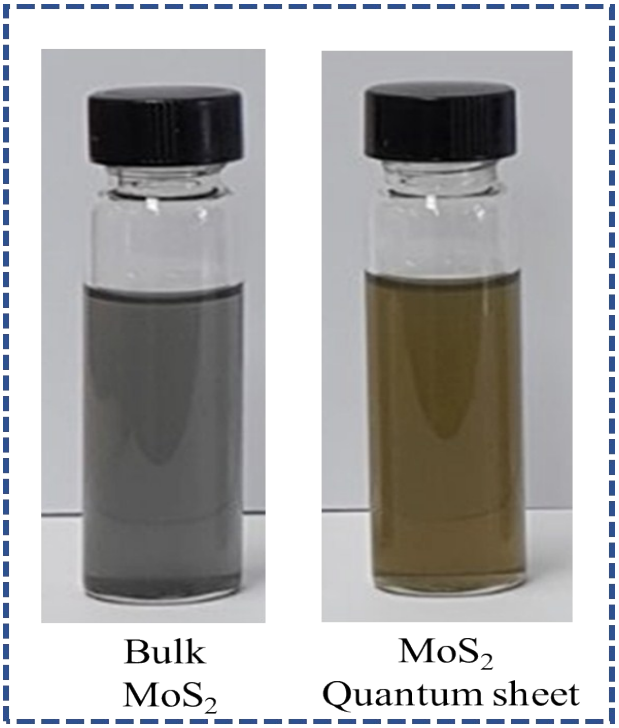

Figure S1: Digital photographs of bulk MoS_2 and MoS_2 quantum sheets dispersed in the DI water.

Figure S1 shows the digital photographs of the bulk MoS_2 (black) and MoS_2 QSs (brownish-green) dispersed in DI water which reveals the significant change in colour of the solutions. This is due to significant quantum confinement in MoS_2 QSs compared to the bulk MoS_2.

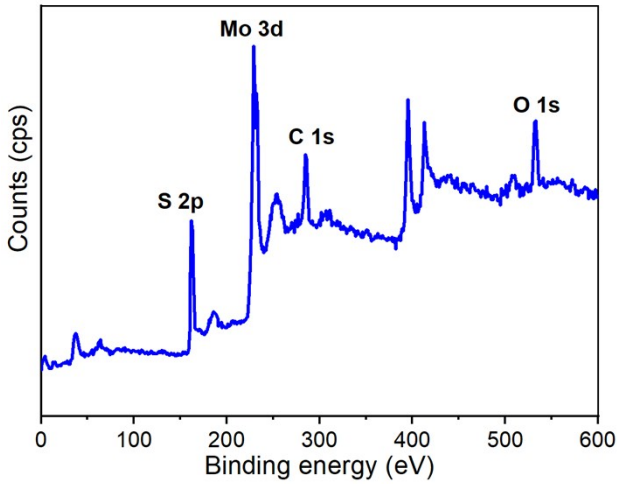

Figure S2. XPS survey spectrum of MoS_2 QSs.

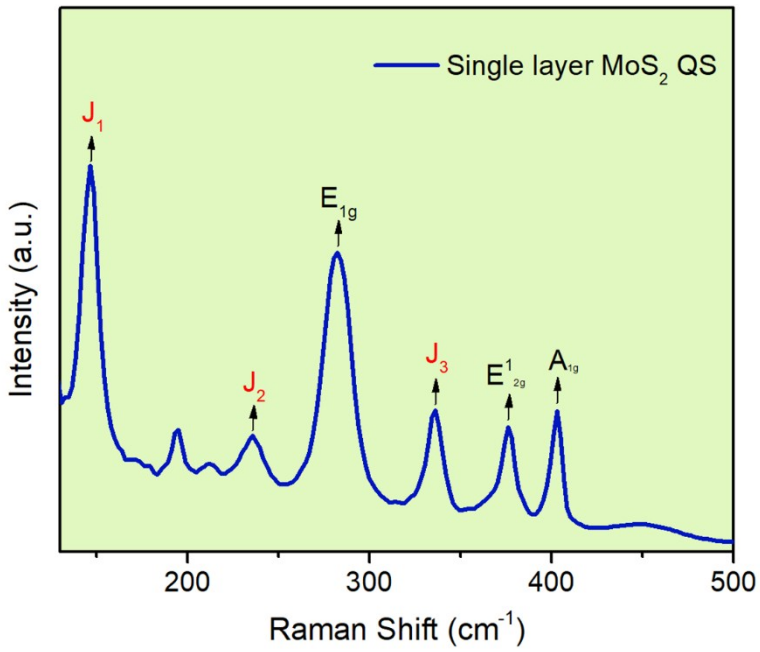

Figure S3. Raman spectrum for the single-layered MoS_2 QSs.

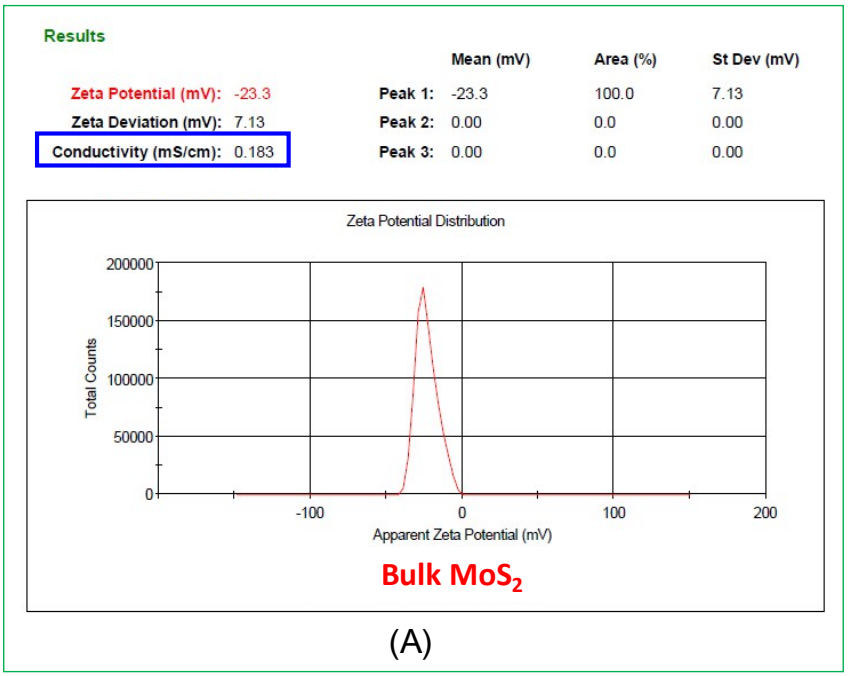

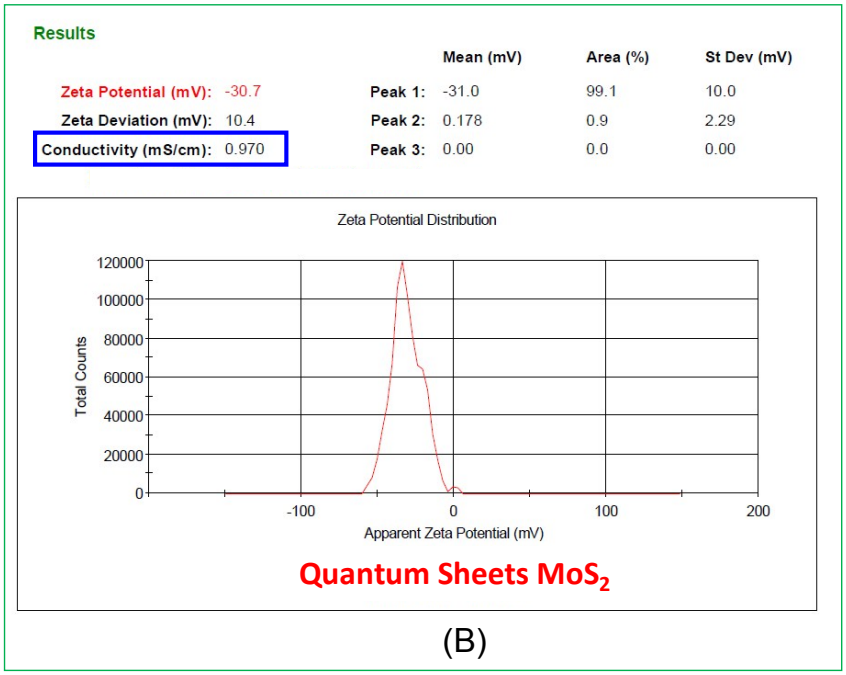

Figure S5. Zeta potential measurements of aqueous dispersions containing bulk MoS_2 and MoS_2 QSs.

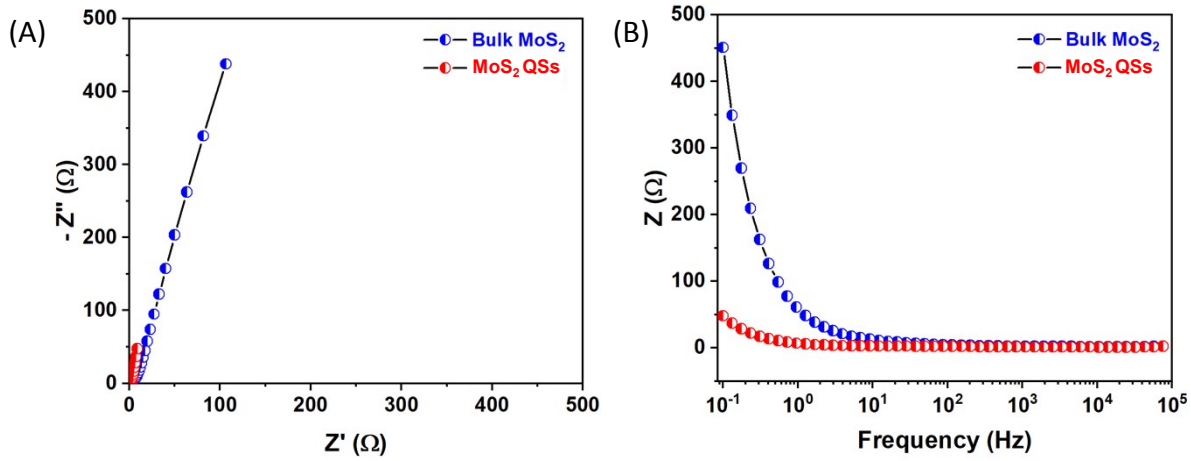

Figure S5. Electrochemical impedance spectroscopy of bulk MoS_2 and MoS_2 QSs electrodes. (A) Nyquist plot (plot of real vs. imaginary impedance) (B) Bode modulus plot (plot of electrochemical impedance vs. applied frequency).

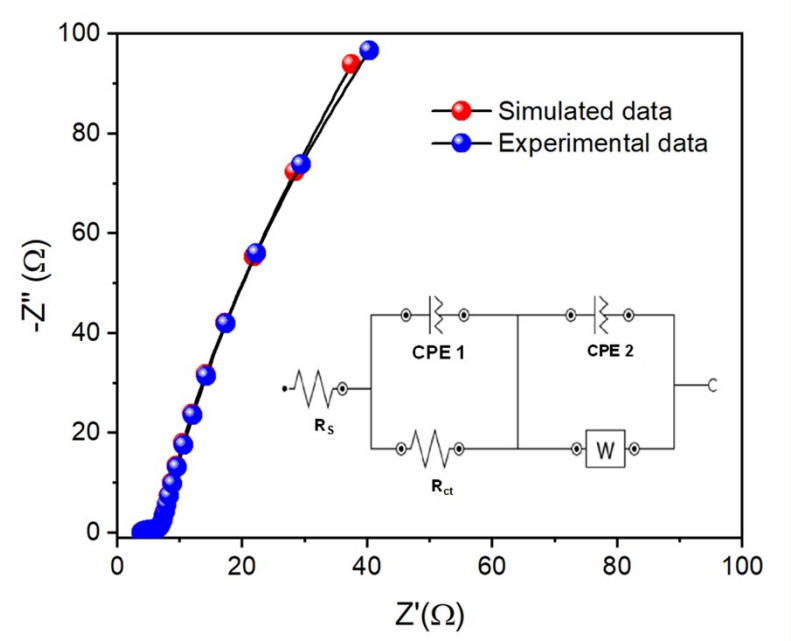

Figure S6. Nyquist plot of MoS_2 QSs based SSC device and the inset presents the corresponding equivalent circuit model.

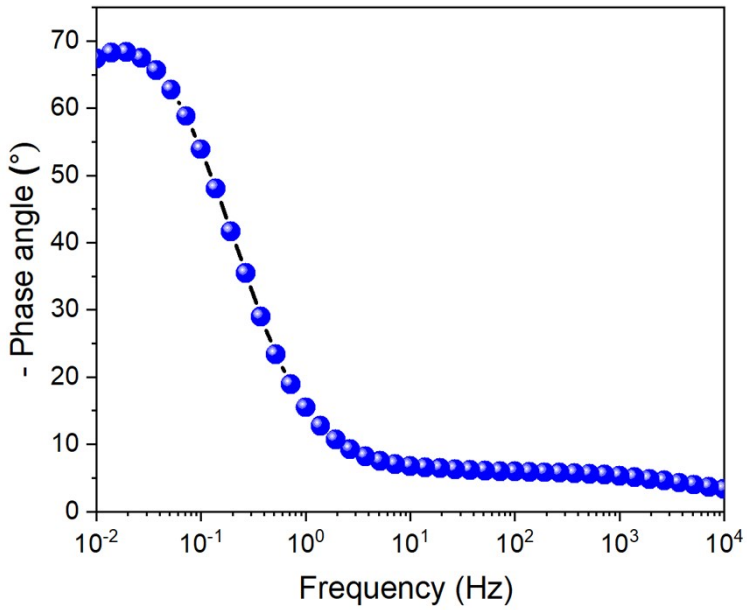

Figure S7: Bode phase angle plot of MoS_2 QSs SSC.

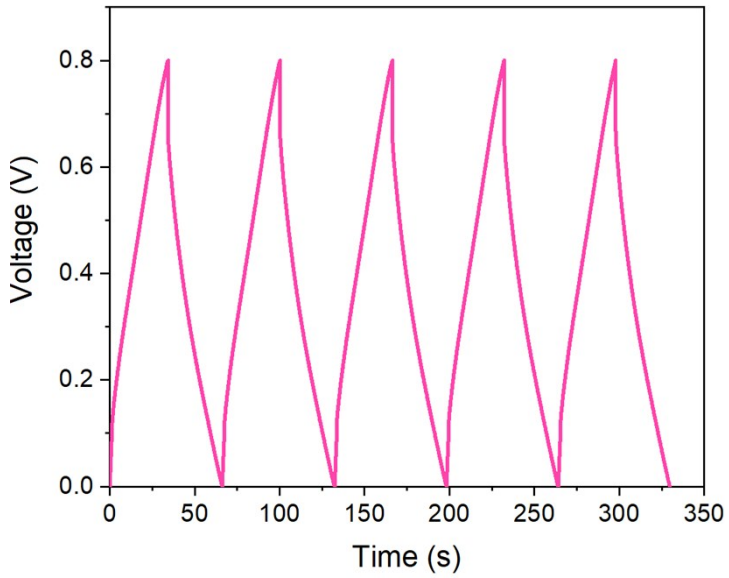

Figure S8. Continuous charge-discharge cycles of MoS_2 QSs SSC measured at a constant current of 5.0 mA.

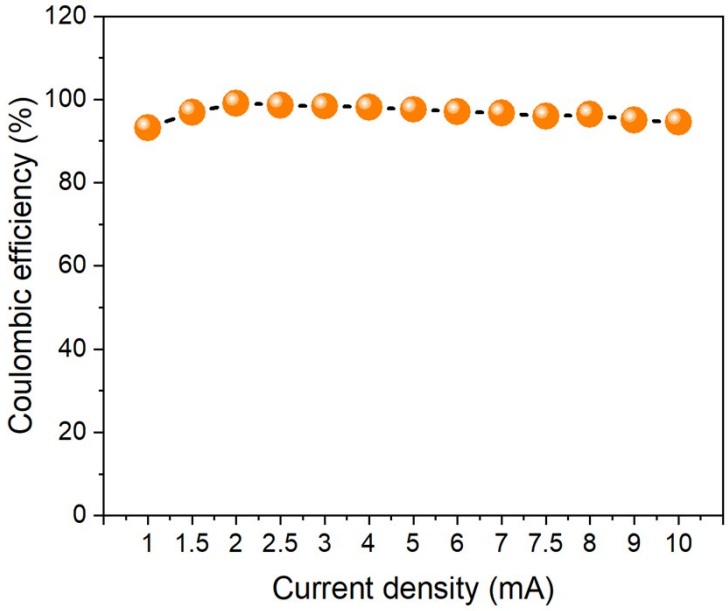

Figure S9: Coulombic efficiency plot of MoS_2 QSs SSC device measured at various current.

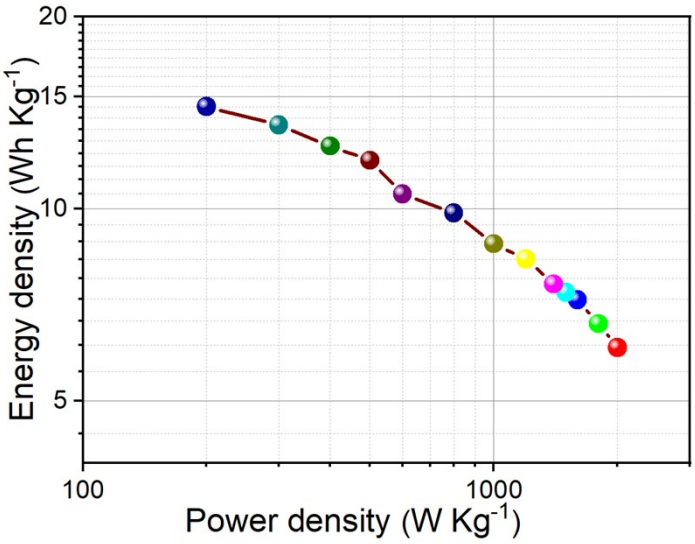

Figure S10. Ragone plot of MoS_2 QSs SSC device.

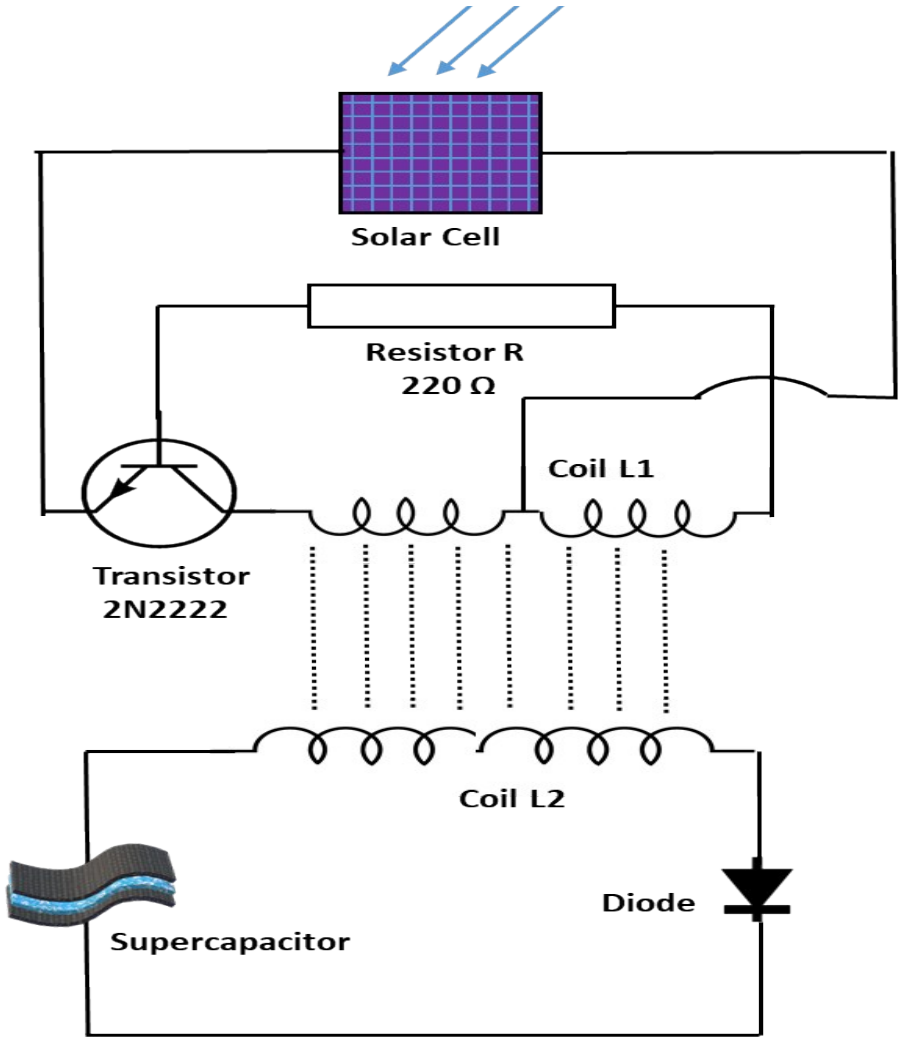

Figure S11. Circuit diagram for solar-driven wireless charging of MoS_2 QSs SSC.

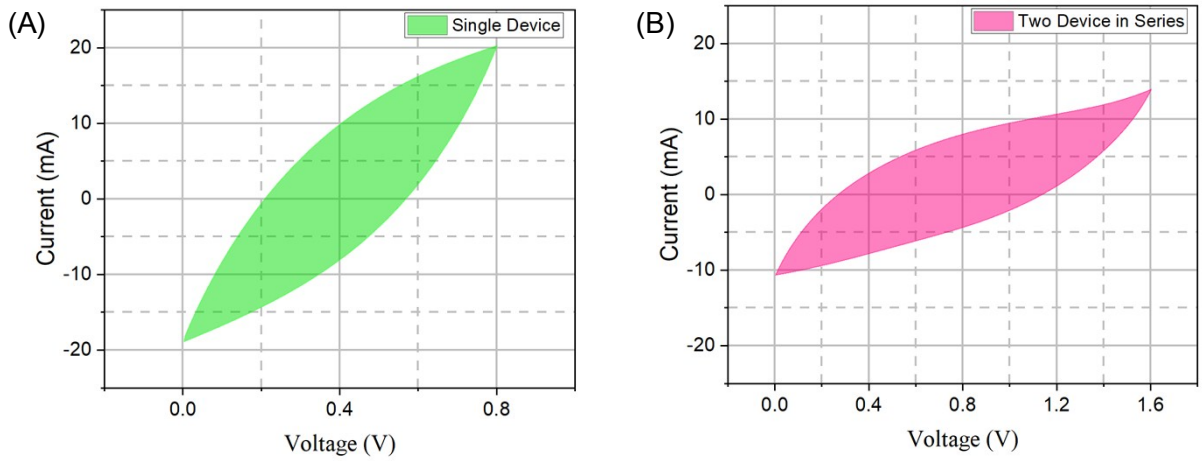

Figure S12: Cyclic Voltammetry (CV) profile for (A) single MoS_2 QSs SSC and (B) two MoS_2 QSs SSC connected in series.

Table 1: Comparison of the rate capability of MoS_2 QS based SSC to that of the reported ones.

S. No	Material name	No. of fold increment in the current density	Capacitance retention (%)	Ref.
1.	MoS_2/RGO/MoS_2@Mo	After (×2.5)	37.5%	[5]
2.	MoS_2-Ni Foam	After (×10)	48.5%	[6]
3.	VSL-MoS_2	After (×3)	50%	[7]
4.	S-MoS_2/CNS	After (×10)	45%	[8]
5.	f-MoS_2/CNS	After (×10)	44%	[8]
6.	Flower-like MoS_2	After (×10)	51.5%	[9]
7.	Siloxene	After (×10)	31%	[10]
8.	WS_2	After (×10)	37%	[11]
9.	MoS_2 QSs	After (×10)	42.5 %	(This work)

Table S2: Performance Metrics of MoS_2 QSs SSC device with reported SSCs using MoS_2 based electrode materials.

S. No	SSC Device	Electrolyte	OPW	Specific Capacitance ($F\ g^{-1}$)	Energy Density ($Wh\ kg^{-1}$)	Power Density ($W\ kg^{-1}$)	Ref.
R1	Commercial MoS_2	-	-	-	0.1	1500	[12]
R2	2H-MoS_2	-	-	-	0.16	1500	[12]
R3	VSL-MoS_2	PVA/Na_2SO_4	0-1.0 V	34.1	4.7	1900	[7]
R4	1T-MoS_2	1 M H_2SO_4	0-0.6 V	-	5	8550	[12]
R5	MoS_2-Ni Foam	PVA/Na_2SO_4	0-1.0 V	38.9	5.4	2800	[6]
R6	MoS_2 Nanospheres	PVA/LiCl	-0.8-0.8V	-	5.42	128	[13]
R7	MoS_2/RGO/MoS_2@Mo	1 M H_2SO_4	0-0.9 V	53.3	6.22	1870	[5]
R8	s-MoS_2/CNS	1M Na_2SO_4	0-0.7 V	108	7.4	3700	[8]
R9	f-MoS_2	1M Na_2SO_4	0-0.8V	96	8.59	4000	[8]
10	MoS_2 QSs SSC	PVA/H_2SO_4	0-0.8V	162.7	14.46	2000	This work

Table S3: Electrochemical performances of 2D MoS_2 QSs based SSC to that of reported flexible supercapacitors at different bending states.

No.	Supercapacitor	Bending state	Capacitance Retention (%)	Ref.
1.	Ag-3D graphene foam (SSC)	10 mm radius	96.77 %	[14]
2.	Graphene aerogel (SSC)	90º	95-100%	[15]
3.	Au-graphene film (SSC)	Compressive bending	98 %	[16]
4.	Ti_3C_2 MXene (ASC)	90º	80 %	[17]
5.	MoS_2-graphene (SSC)	High bend state	Slight reduction	[18]
6.	1T MoS_2 nanosheet (SSC)	180º	94.9 %	[19]
7	1T MoS_2 QSs (SSC)	180º	98 %	This work

References

1 C. Han, Y. Zhang, P. Gao, S. Chen, X. Liu, Y. Mi, J. Zhang, Y. Ma, W. Jiang and J. Chang, *Nano Letters*, 2017, **17**, 7767–7772.

2 J. W. Park, W. Na and J. Jang, *Journal of Materials Chemistry A*, 2016, **4**, 8263–8271.

3 K. Krishnamoorthy, S. M. S. P., P. Pazhamalai, V. K. Mariappan, Y. S. Mok and S.-J. Kim, *Journal of Materials Chemistry A*, 2019, **7**, 18950–18958.

4 S. Sahoo, K. Krishnamoorthy, P. Pazhamalai, V. K. Mariappan, S. Manoharan and S. Kim, , DOI:10.1039/c9ta06245a.

5 Y. Zhang, P. Ju, C. Zhao and X. Qian, *Electrochimica Acta*, 2016, **219**, 693–700.

6 R. K. Mishra, M. Krishnaih, S. Y. Kim, A. K. Kushwaha and S. H. Jin, *Materials Letters*, 2019, **236**, 167–170.

7 R. K. Mishra, A. K. Kushwaha, S. Kim, S. G. Seo and S. H. Jin, *Current Applied Physics*, 2019, **19**, 1–7.

8 T. N. Y. Khawula, K. Raju, P. J. Franklyn, I. Sigalas and K. I. Ozoemena, *Journal of Materials Chemistry A*, 2016, **4**, 6411–6425.

9 F. Wang, G. Li, J. Zheng, J. Ma, C. Yang and Q. Wang, *RSC Advances*, 2018, **8**, 38945–38954.

10 P. Pazhamalai, K. Krishnamoorthy, S. Sahoo and S. J. Kim, *Electrochimica Acta*, 2019, **295**, 591–598.

11 N. Islam, S. Wang, J. Warzywoda and Z. Fan, *Journal of Power Sources*, 2018, **400**, 277–283.

12 S. Yang, K. Zhang, C. Wang, Y. Zhang, S. Chen, C. Wu, A. Vasileff, S. Z. Qiao and L. Song, *Journal of Materials Chemistry A*, 2017, **5**, 23704–23711.

13 M. S. Javed, S. Dai, M. Wang, D. Guo, L. Chen, X. Wang, C. Hu and Y. Xi, *Journal of Power Sources*, 2015, **285**, 63–69.

14 L. Manjakkal, C. G. Núñez, W. Dang and R. Dahiya, *Nano Energy*, 2018, **51**, 604–612.

15 D. W. Kim, S. M. Jung and H. Y. Jung, *Journal of Materials Chemistry A*, 2020, **8**, 532–542.

16 K. Yang, K. Cho, D. S. Yoon and S. Kim, *Scientific Reports*, 2017, **7**, 2–9.

17 Z. Zhang, M. Guo, Y. Tang, C. Liu, J. Zhou, J. Yuan and J. Gu, *Nanotechnology*, 2020, **31**, 165403.

18 F. Clerici, M. Fontana, S. Bianco, M. Serrapede, F. Perrucci, S. Ferrero, E. Tresso and A. Lamberti, *ACS Applied Materials and Interfaces*, 2016, **8**, 10459–10465.

19 X. Wang, W. Ding, H. Li, H. Li, S. Zhu, X. Zhu, J. Dai, Z. Sheng, H. Wang, X. Zhu, Y. Sun and S. X. Dou, *Journal of Materials Chemistry A*, 2019, **7**, 19152–19160.